Accurate calculations of the ground state and low-lying excited states of the (RbBa)+ molecular ion: a proposed system for ultracold reactive collisions

S Knecht, L K Sørensen, H J Aa Jensen, Timo Fleig, C M Marian

Accurate calculations of the ground state and low-lying excited states of the $(RbBa)^+$ molecular ion, a proposed system for ultracold reactive collisions

S Knecht[1], L K Sørensen[1], H J Aa Jensen[2], T Fleig [3], and C M Marian[1]

[1] Theoretical and Computational Chemistry, Heinrich Heine University Düsseldorf, Universitätsstraße 1, D-40225 Düsseldorf, Germany

[2] Department of Physics and Chemistry, University of Southern Denmark, DK-5230 Odense M, Denmark

[3] Laboratoire de Chimie et Physique Quantiques, I.R.S.A.M.C., Université Paul Sabatier, Toulouse III, route de Narbonne 118, 31062 Toulouse Cedex 04, France

E-mail: sknecht@unistra.fr,lasse@theochem.uni-duesseldorf.de, hjj@ifk.sdu.dk,timo.fleig@irsamc.ups-tlse.fr,cm@theochem.uni-duesseldorf.de

Abstract. Collisions of ultracold Ba^+ ions on a Rb Bose-Einstein condensate have been suggested as a possible benchmark system for ultracold ion-neutral collision experiments. However, *a priori* knowledge of the possible processes is desirable. For this purpose we here present high-level four-component coupled cluster and multi-reference configuration interaction calculations of potential energy curves, dipole moments, and spectroscopic constants of the experimentally interesting low-lying electronic states of the $(RbBa)^+$ molecule. Our results show significant avoided crossings between the $^3\Sigma^+_{1,0^-}$ Rb + Ba^+ entrance channels and low-lying charge transfer $^3\Pi_{1,0^-}$ states of the Rb^+ and $Ba_{6s^15d^1}(^3D)$ atomic channels, indicating that a fast non-radiative charge transfer is possible. Population analysis shows that a partially covalent polar bond is formed in the ground state, which thus deviates significantly from a pure Rb^+ + Ba interaction. This finding is corroborated by the electric dipole moment which is found only to be 4.5 D at the equilibrium bond distance, compared with the 14 D for a pure Rb^+ + Ba interaction, thereby supporting the view of a partial charge transfer between the two atoms.

PACS numbers: 31.15.ae, 31.15.ag, 31.15.aj, 31.15.am, 31.15.bw, 31.15.vj, 31.15.vn, 33.15.Fm, 34.70.+e

Submitted to: *J. Phys. B: At. Mol. Opt. Phys.*

1. Introduction

The study of reactive collisions at very low temperatures (below 1 μK) is a promising new direction in the field of cold and ultracold quantum matter. This temperature regime provides a unique environment to investigate, *inter alia*, the quantum mechanical details of chemical reactions, ultimately aiming at a controlled chemistry at the quantum level [1]. Other interesting prospects concern the possibility of testing fundamental symmetries in nature [2, 3] or the spacetime independence of electron and nuclear masses [4].

Ion-neutral interactions are distinguished from neutral-neutral collisions in that the interaction of the former is long-range, in general leading to large collision cross sections [5, 6] and entailing the possibility of charge transfer between the collision partners [7]. Many experimental and theoretical studies of ion-neutral reactions exist, but the low-energy regime has only been addressed recently, *e.g.* in references [5, 8, 9]. Due to the complexity of the *ab initio* electronic-structure calculations needed to compute accurate short-range potentials, most of these studies considered few-electron systems [6]. The few published investigations on many-electron systems involving a cationic reaction partner, such as the studies on $(NaNa)^+$ and $(NaCa)^+$ [7, 10], employ rather approximate potentials involving parameters taken from experiment.

Other aspects of ion-neutral collisions than charge-transfer processes have also received attention. An intriguing case is the formation of a predicted mesoscopic molecular bound state arising from a single trapped ion in a sea of ultracold atoms [11]. In this context, J. Hecker Denschlag has suggested that very low energy collisions of Ba^+ ions with a Bose-Einstein condensate of neutral Rb atoms could be a benchmark system, provided accurate electronic potential energy curves and collision kinetics were calculated for $(RbBa)^+$[12]. The $(RbBa)^+$ system is valence isoelectronic with the $(MgK)^+$, $(MgCs)^+$, and $(NaCa)^+$ systems which have been considered in earlier experiments [10, 13, 14]. The associated theoretical investigations were mainly carried out using large-core pseudopotentials and neglecting spin-orbit coupling. In these three systems, the lowest-lying electronic states are characterized as Σ states, which is also true for the $(RbBa)^+$ molecular ion [15] and most likely also for another heavier species of interest, $(MgCs)^+$. The neglect of spin-orbit interaction is reasonable in the determination of such Σ states, since it affects these states only through higher-order couplings to excited states of different angular momentum projection Λ (M_L) onto the internuclear axis. In the energy regime close to the $Rb_{5s^1} + Ba^+_{6s^1}$ entrance channel one would expect a rich manifold of low-lying excited states with angular momentum projection greater than zero ($\Lambda > 0$) based on the atomic excitation energies and ionization potentials. This was confirmed by the calculations in Ref. [15] where the nine lowest-lying molecular electronic states of the $(RbBa)^+$ ion were calculated employing a spinfree Hamiltonian [16]. The obtained $\Lambda - S$ states split into their Ω (M_J) components when spin-orbit coupling is taken into consideration. Since the $\Lambda > 0$ states in the spinfree approximations are possible candidates for a charge transfer from Ba^+ to Rb,

which could lead to a transition to the electronic ground state, it is therefore essential to account properly for the various Ω components of these states to aid the interpretation of ongoing experiments [12].

Since two heavy atoms are involved we apply quantum-chemical methods which treat electron correlation and relativistic effects on the same footing. Relativistic coupled cluster (CC) and configuration interaction (CI) approaches are used in a complementary fashion, the details of which are described in the following section. In the main body of the paper (section 3) we first embark on a systematic study of what is needed to achieve high accuracy for the ground states and relevant excited states of the two atoms as well as for the potential energy curve of the electronic ground state of $(RbBa)^+$. Based on these results we designed our final multi-reference configuration interaction (MRCI) model such that the calculations become feasible and also deliver accurate spectroscopic values for the states in question and, furthermore, describe well the relevant avoided crossings of the potential curves. We present and discuss the electronic molecular potentials obtained with this MRCI model and point to possible radiative as well as non-radiative charge-transfer processes which can occur. We also investigate the ground state dipole moment as a function of distance to visualize effects of any covalent character in the ground state. In the final section we summarize and draw conclusions.

2. Theory and Computational Details

2.1. Hamiltonian operator

Spin-orbit interactions are accounted for in the rigorous four-component relativistic framework by using the Dirac-Coulomb Hamiltonian

$$\hat{H}_{DC} = \sum_i \left(c\hat{\vec{\alpha}}_i \cdot \hat{\vec{p}}_i + mc^2\hat{\beta} + \sum_A \hat{V}_{iA}^{nuc} \right) + \frac{1}{2}\sum_{i\neq j} \mathbf{1_4}\frac{1}{r_{ij}}. \quad (1)$$

All classes of two-electron integrals of this Hamiltonian in the 4-spinor basis were included, namely the integrals involving four large-component indices $\langle LL|LL\rangle$, large- and small-component indices as $\langle LL|SS\rangle$, and four small-component indices $\langle SS|SS\rangle$; except where otherwise noted. The spinfree Hamiltonian used here is defined by a projection of the full Dirac-Coulomb Hamiltonian [16, 17], by which all spin-dependent terms are removed. Therefore, no perturbation parameters are required for the separation into spinfree and spin-dependent terms (as for e.g. the Breit-Pauli Hamiltonian), and the spinfree Hamiltonian is thus in this sense exact. Both Hamiltonians and the implementations of them in the `DIRAC` program package are described in reference [18].

2.2. Electron Correlation Methods

Calculations of sufficiently accurate ground- and excited-state wave functions along with vertical and adiabatic excitation energies became feasible with the recent parallelization

[19, 20] of the relativistic double group large-scale MRCI program LUCIAREL[21, 22, 23]. Configuration interaction (CI) theory is based on a linear parametrization of the wave function Ψ_k through an expansion in a set of M N-particle functions Φ_i, *in casu* Slater determinants built from Hartree-Fock orbitals:

$$\Psi_k = \sum_{\mu=0}^{M} c_{\mu k}\Phi_i = (c_{0k}\hat{1} + \sum_{\mu=1}^{N} c_{\mu k}\hat{\tau}_\mu)\left|\Psi^{\mathrm{RHF}}\right\rangle \tag{2}$$

Using the Rayleigh-Ritz variation principle, this leads to a matrix eigenvalue problem for the Hamiltonian $\hat{H}$, *e.g.* $\hat{H}_{DC}$ (see Eq. (1)),

$$\mathbf{H}\mathbf{c}_k = E_k\mathbf{c}_k, \tag{3}$$

where $\mathbf{c}_k$ is the CI coefficient vector and E_k the corresponding eigenvalue. There are no principle restrictions on which excitation levels (singles, doubles, triples, ...) to include in the $\hat{\tau}_\mu$ excitation operators, the only real restriction is how big a dimension M is feasible with your computational resources.

The other method used in this work, the single reference coupled-cluster (CC) theory, is based on an exponential parametrization of the wave function which gives fast convergence of the electron correlation energy with respect to the excitation level used in the cluster operators [24]. A set of projection equations

$$\left\langle \Psi^{\mathrm{RHF}} \left| e^{-\hat{T}}\hat{H}e^{\hat{T}} \right| \Psi^{\mathrm{RHF}} \right\rangle = E_{CC} \tag{4}$$

$$\left\langle \mu \left| e^{-\hat{T}}\hat{H}e^{\hat{T}} \right| \Psi^{\mathrm{RHF}} \right\rangle = 0 \tag{5}$$

$$\hat{T} = \sum_{\mu=1}^{N} t_\mu\hat{\tau}_\mu = \sum_{\mu=1}^{N}\hat{T}_\mu \tag{6}$$

is solved, yielding the CC energy E_{CC} and an optimized set of cluster amplitudes $\{t_\mu\}$. The truncation of the cluster operator for the CCSD method is performed at the doubles level of excitation,

$$\hat{T} = \hat{T}_1 + \hat{T}_2. \tag{7}$$

The linear CI method is a straightforward approach to describe any multiconfiguration open-shell state and to include dynamic correlation in the wave function after the Hartree-Fock step, provided the calculation is doable (M not too big). Unfortunately the dynamic correlation is slowly converging with the dimension M. How is large-scale CI calculations made feasible? Since in most cases only a small sub-set $\{\Psi_k\}, k \in \{1, \ldots, m\}$ of all M solutions is needed, iterative sub-space diagonalization schemes were proposed [25, 26, 27] to reduce the computational scaling from roughly M^3 to M^2. And as most pairs among the M Slater determinants differ by more than two spinors, the CI Hamiltonian matrix $\mathbf{H}$ is very sparse, and use of this sparsity reduces the computational scaling further to nM where $n \ll M$ when M is large. Good use of these two aspects is what makes large-scale accurate CI calculations feasible in some quantum-chemistry codes. The parallelized LUCIAREL CI program code is able to routinely handle very large CI expansions ($M > 10^9$ determinants) on standard Linux-based clusters. It will be

made available in the next release of the DIRAC program package [28]. By exploiting the generalized active space (GAS) concept [21] in the CI, a flexible correlation treatment of multiconfigurational states of any symmetry is possible. The orbital space can be divided into any number of sub-orbital spaces and any restrictions can be imposed on the allowed excitations between these sub-orbital spaces. The Ω quantum number for a given electronic state has been assigned by calculating its expectation value of the $\hat{j}_z$ operator [20].

The convergence of the dynamical correlation in the MRCI method is, however, slow with respect to the excitation level. In contrast, the non-linear single-reference CC method converges fast with respect to dynamical correlation, but is poor in describing states not dominated by a single configuration. Therefore we also performed CCSD(T) calculations on the closed-shell ground state to validate the accuracy of the treatment of dynamical correlation in the MRCI calculations. In the study of the ground-state properties we used the RELCCSD module [29, 30], which can perform coupled cluster singles doubles (CCSD) and perturbative triples (CCSD(T)) calculations, and is available in the DIRAC08 quantum chemistry program package [28]. Since the only important relativistic contribution for the ground state of $(RbBa)^+$ is expected to be scalar relativistic (in other words: spin-orbit effects are expected to be negligible compared to desired accuracy), we employed in the CC equations the computationally cheaper spinfree Dirac-Coulomb Hamiltonian by Dyall [16] in the ground-state calculations.

2.3. Setup of the Calculations

In the coupled-cluster treatment we correlated the Rb $4p^6$ and the Ba $5p^6$ outer-core electrons in addition to the Ba $6s^2$ valence electrons. Recent studies on LiCs [31] showed that correlation of the core $4d$ shell on Cs has very little impact on the spectroscopic values of LiCs, and we therefore infer that it is safe to neglect correlation of the $3d$ shell on Rb and the $4d$ shell on Ba. The LiCs study also revealed that correlating the energetically lower-lying $5s$ outer core on Cs contracted the bond by about 0.02 bohr which is unimportant. We therefore concluded that in the present study it is not necessary to include the outer core $4s$ on Rb and $5s$ Ba in the correlation treatment. Along the entire potential energy curve we used closed-shell spinfree Dirac-Coulomb Hartree-Fock (SF-DCHF) for the generation of molecular spinors. This set of spinors was employed since the ground state is dominated by a single determinant.

In the MRCI calculations we included the Rb $5s5p$ and the Ba $5d6s6p$ spinors (of which only Ba $6s$ is formally occupied in the ground state) in the active space, yielding a distribution of two valence electrons in 13 Kramers pairs. Single holes in the Rb $4p$ and Ba $5p$ shells were included to describe outer-core polarization, and single and doubles into energy-selected virtual spinors (see section 2.4) were included to account for dynamic electron correlation. In our notation we dub this computational scheme S12_(2in13)_SD which follows the notation of GAS1_(GAS2)_GAS3 laid out in

an earlier publication [32]. The ensuing CI expansion comprises approximately 5×10^6 determinants. As for the CC calculations the molecular spinors have been obtained from a closed shell DCHF.

2.4. Basis sets and basis set superposition error

All calculations were four-component performed with large-component basis sets consisting of uncontracted scalar Gaussian type orbitals (GTO). The small-component basis functions were generated by the restricted kinetic balance condition [18]. The charge induced dipole interaction and the London dispersion contribution to the long-range part of the potential are not adequately described in our MRCI calculations and we therefore refrain from extracting the C_n coefficients from the asymptotic behavior and calculating the scattering length [33]. For all the ground-state coupled-cluster calculations we used extended triple zeta (TZ) basis sets by Dyall [34]. For Rb our $(29s21p15d2f)$ basis set is Dyall's TZ basis set extended with correlating and polarizing functions [34] for the valence and the outer-core $4s4p$ shells. This choice of basis set has been shown to perform well in a recently published paper on RbYb [32]. For Ba we added Dyall's correlating and polarizing functions for the valence and the outer-core $5s5p$ shells to form an $(31s25p18d3f)$ extended TZ basis set. The polarizing functions were added to ensure accurate dipole moments for the electronic ground state.

For the MRCI calculations, where the focus was on proper treatment of all low-lying excited states, we followed the scheme in Ref. [35], and the Ba basis set was further augmented with a d, an f, and a g function with exponents of 0.036645714, 0.3000341, and 0.76354824, respectively. This was done in order to properly describe excitations to the Ba $5d$ shell which plays a crucial role in the charge transfer from Rb to Ba^+ and could enable a transition to electronic ground state. On the other hand, no dipole moments or other electric properties were envisaged to calculate with the MRCI and therefore the polarizing functions for the outer-core shells Rb $4s4p$ and Ba $5s5p$ were not included. This setup results in a total of $(28s20p14d1f)$ for Rb and $(30s24p18d3f1g)$ for Ba which is the basis set used in all present MRCI calculations.

The energy threshold for the truncation of the virtual spinors in the final correlated calculations was set at 18 Hartree. The validity of this choice was confirmed by calculating the complete potential energy curve of the ground state at the spinfree CCSD and CCSD(T) levels with a truncation of the virtual spinors at 42 Hartree as well. As seen from the results in Table 1, the differences in the spectroscopic parameters between the 18 and 42 Hartree truncations are more than a factor of 100 smaller than the differences between CCSD and CCSD(T).

The basis set superposition error (BSSE) in the electronic ground state was accounted for by applying the counterpoise (CP) correction as suggested by Boys and Bernardi [36].

2.5. Dipole moments

Dipole moments along the ground state potential energy curve were calculated using the finite-field technique by varying the electric field along the bond axis (chosen as z). For the dipole moment a seven-point numerical derivative has been shown in previous publications [32, 31] to yield sufficiently accurate results and will therefore also be employed here. The field strengths used were ± 0.0001, ± 0.0002, and ± 0.0004 Hartree $e^{-1}\,bohr^{-1}$ to form the numerical derivative of the energy with respect to the electric field taken at zero field strength. While in a neutral molecule the calculated dipole moment is independent of the choice of the origin of the coordinates, this is not the case for an ionic system. In agreement with conventions, the origin of the molecular coordinate system was chosen to lie in the atomic center of mass. In this way we could calculate the dipole moment at different internuclear distances with the WFFIT program by Sadlej [37], and this has been done at the CCSD and CCSD(T) levels of theory for the ground state.

3. Results

Table 2 gives an overview of the atomic configurations and terms as well as their corresponding molecular states that form the lower part of the electronic spectrum of the $(RbBa)^+$ molecular ion up to ≈ 14000 cm^{-1} above the ground state. These molecular states include also the Σ states correlated with the entrance channel for the envisaged collision experiments involving an ultracold ionized trapped barium atom and a Bose-Einstein condensate of neutral rubidium atoms. In the following we shall elaborate on our results for all the molecular states located below the entrance channel plus the d channels associated with the $Rb^+_{5s^0}(^1S_0)$ + $Ba_{6s^1 5d^1}(^3D_{1,2,3}\ ;\ ^1D_2)$ atomic limits listed in Table 2. As our results discussed in Section 3.3 show, notable interactions between electronic states of the same Ω quantum number are observed for the molecular states correlating with these channels. We therefore predict that radiative as well as non-radiative transitions will play a crucial role in the charge transfer process from Rb + Ba^+ to Rb^+ + Ba and for the lifetime of the different states in the excited-state manifold.

3.1. Atomic calculations and ionization potentials

In Table 3 we have compiled our results of atomic and atomic-like excitation energies of the lowest Ba atomic transitions as well as previous theoretical work and experimental data. Comparison of our atomic MRCI S6_(2in9)_SD and the atomic-like molecular MRCI S12_(2in13)_SD results indicates that the dissociation limit is reached at an internuclear separation of 50 bohr. From previous studies on transition metals it is known that $ns^2(n\text{-}1)d^m \rightarrow ns^1(n\text{-}1)d^{m+1}$ excitations are difficult to describe in general within an MRCI approach because of the slow convergence of the dynamical electron correlation contributions [38]. Multi-reference CC approaches, such as for example the Fock-space CCSD (FSCCSD) or the intermediate Hamiltonian IHFSCCSD methods

[39, 40, 41], are better at describing dynamical electron correlation energies. They are therefore expected to yield closer agreement with experiments, as the results in Table 3 confirm. In view of these difficulties the deviations of our computed ^{3}D and ^{1}D MRCI excitation energies from the experimental values on the order of a few 100 cm^{-1} are satisfactory. The fine-structure splittings of these terms are even reproduced within a few tens of cm^{-1}(see Table 3). Moreover, the good agreement of our calculated $Ba_{6s^16p^1}(^3P)$ excitation energies with experiments shows that the chosen basis set and correlation treatment are adequate.

In addition to the energetic location of the low-lying neutral Ba channels, the differential ionization potential of Rb and Ba is of vital importance for an unbiased description of the $(RbBa)^+$ molecular states. Our computed ΔIP = IP(Ba) - IP(Rb) value of 8454 cm^{-1} is in excellent agreement with experiment (8344 cm^{-1}) [42]. This ΔIP was calculated as the excitation energy in the atomic-like limit at 50 bohr of a molecular calculation. The Ba^+ + Rb entrance channel is thus only slightly below the $Ba_{6s^15p^1}(^3D_1)$ + $Rb^+_{5s^0}$ atomic channel. This is in contrast to the lighter homologous $(NaCa)^+$, $(MgK)^+$ and $(MgCs)^+$ where the corresponding energy gap is much larger.

3.2. Ground state potential and bonding analysis

In Table 4 we report our calculated MRCI spectroscopic constants for the $^1\Sigma^+_{0^+}$ ground state of $(RbBa)^+$ and compare with values derived from our four-component as well as spinfree CCSD and CCSD(T) calculations. The spin-orbit effect on the ground state potential was found to be well within the expected error bounds for the spectroscopic properties at CC level. We therefore consistently used the spinfree Hamiltonian for the ground-state dipole-moment calculations (see section 3.4) since the time consuming part in the CCSD and CCSD(T) with the DC Hamiltonian is the coupling of all spin projections M_S needed to describe the — in this case — negligible spin-orbit contribution to the electronic potential.

In agreement with the findings of an earlier study on RbYb [32], counterpoise correction has only a minor effect on the spectroscopic constants of the ground state. Inspecting Table 4, it is comforting that the present spin-dependent MRCI S12_(2in13)_SD approach compares favorably to the more sophisticated CCSD(T) method. The deviation of 0.03 bohr in the equilibrium bond distance R_e is small for such a weakly-bound molecular ion with R_e = 8.75 bohr. Moreover, the harmonic frequency ω_e as well as the dissociation energy D_e agree perfectly with the CCSD(T) values. The differences between the older spinfree [15] and the presented spin-dependent MRCI results are mainly attributed to AO basis set effects since in the spinfree case an ANO-RCC basis set with a truncation of the virtual space at 5 Hartree was used. As could be expected for a "Σ" state, spin-orbit coupling hardly affects the calculated spectroscopic parameters as seen in the CC calculations. In contrast, we see a substantial reduction of the equilibrium distance and an increase of the dissociation energy by about 150 cm^{-1} when triple excitations are included perturbatively in the CC treatment. This finding is

in line with what has also been observed for other weakly bound systems like LiCs [31] and RbYb [32] where a CCSD treatment was also found to be insufficient.

In the MRCI expansion the ground state is dominated by the reference determinant which has a CI coefficient of 0.94 around equilibrium. A Mulliken population analysis of the underlying DCHF wave function reveals that the highest occupied molecular orbital (HOMO) is not a purely atomic Ba 6s Kramers pair. The Ba 6s spinors are populated by only 1.5 electrons. Roughly 0.4 electrons have been transferred to a Rb σ-type orbital. The remaining 0.1 electrons reside in the Ba $5d_\sigma$ that is also involved in the binding. The second largest CI coefficient of about -0.1 is found for the double excitation to the lowest unoccupied molecular orbital (LUMO), which the Mulliken population analysis again reveals to be significantly mixed. The LUMO is composed of Rb $5s(0.613)$, Ba $6p_z(0.209)$, $6s(0.150)$, and $5d_{xx}$, $5d_{yy}(0.011)$. We furthermore see many single and double excitations to molecular spinors which are made up of Rb 5s and 5p and Ba 6s, 6p, and 5d atomic spinors. This large mixing of the atomic spinors is what led to the choice of including all these spinors in the active space of the MRCI calculations. We are, therefore, confident that the MRCI calculations with this active space perform well for the low-lying states. Of course, upon dissociation the HOMO becomes more and more atomic and locates on Ba.

The mixing with the Rb 5s and 5p in HOMO also means that the ground state cannot be considered to be just a charge-induced dipole $1/R^4$ interaction between Rb^+ and Ba but that there is a significant amount of the valence electron density residing on the Rb atom. The charge transfer is perhaps not so large that one would talk about a bond in a chemical sense but we find that the bond is significantly stronger than what would be expected from a charge-induced dipole interaction. With a dissociation energy of around 5000 cm^{-1} (see Table 4) this is in fact directly comparable to the dissociation energy of the LiCs alkali dimer where D_e is measured to 5875.455 cm^{-1} [43]. The picture of a partially covalent polar bond is also confirmed by the dipole moment which is significantly influenced by the charge distribution in the molecule (see Section 3.4).

3.3. Excited state potentials

In contrast to the ground state, accounting for spin-orbit coupling in the excited states clearly yields a more complex picture for the potential energy curves of the electronically excited states of the molecular ion $(RbBa)^+$ compared to spinfree calculations (compare Fig. 2 with Fig. 7 in [15]). The avoided crossings between the $^3\Sigma^+_{0^-}$ and $^3\Pi_{0^-}$ states as well as the $^3\Sigma^+_1$ and $^3\Pi_1$ states are easily discernible in Figure 1 and in the enlargement of the critical region in Figure 2. Of course, in the spinfree calculations all these curves cross, and it is thus evident that a proper treatment of spin-orbit coupling is mandatory for an explanation and prediction of outcomes of ultracold reactive collisions of Ba^+ on a Rb Bose-Einstein condensate. An even more pronounced avoided crossing between the $^1\Sigma^+$ of the entrance channel and the $^1\Sigma^+$ of the $Ba_{6s^15d^1}(^1D)$ channel is also visually

identifiable in Figure 1. Unlike the above mentioned avoided crossings this one would also be present in a non-relativistic or scalar relativistic calculation. The spin-orbit splittings of the calculated scalar-relativistic states are sizable, in particular for the $^3\Delta$ and $^3\Pi$ states which are split into their $\Omega = 1, 2, 3$ and $\Omega = 0^+, 0^-, 1, 2$ components (see Figure 1 and Table 5). While some of the Ω components are degenerate in the atomic limit because they belong to the same atomic J level, the molecular field gives a spin-orbit splitting also of these components. In addition to the spin–orbit splitting of the spatially degenerate triplets substantial off-diagonal interactions are observed.

Most of the electronically excited states exhibit strong multiconfigurational character and are thus more difficult to interpret in a molecular orbital picture. We will therefore discuss their electronic structure in a more qualitative way. The lowest excited $\Omega = 0^-$ and $\Omega = 1$ states correlate to a $^3\Sigma^+$ state in the Λ-S representation (see Table 2). In the dissociation limit their electronic structure corresponds to Ba^+ + Rb. At shorter nuclear distances more and more $Ba_{6s^1 5d^1_\sigma}(^3D)$ character is mixed in. In the Franck-Condon region the wave function has nearly equal contributions from these two configurations. The fine-structure splitting of its Ω sublevels is a second-order effect that is mainly brought about by the spin–orbit interaction with the close-by $^3\Pi$ state. At about 7.75 bohr the $^3\Sigma^+$ components undergo an avoided crossing with the $\Omega = 0^-$ and $\Omega = 1$ of that $^3\Pi$ state (see Figure 2). This non-adiabatic interaction between the $^3\Sigma^+_{1,0^-}$ and $^3\Pi_{1,0^-}$ states is expected to lead to a non-radiative charge transfer from the $^3\Sigma^+_{1,0^-}$ entrance channel to the $^3\Pi_{1,0^-}$ states. While transition from the $^3\Pi_{1,0^-}$ states to the ground state in $(RbBa)^+$ is also in a scalar-relativistic approximation electric dipole and spin forbidden, the large mixing of the Ba $5d_\pi$ with the energetically close lying Ba $6p_\pi$ and Rb $5p_\pi$ spinors induced by spin-orbit coupling will greatly decrease the radiative lifetime. As a result of the strong admixture of p_π character into the Ba $5d_\pi$ spinors the Ω components of the $^3\Pi$ state display a significantly shorter equilibrium distance than the other states originating from the $Ba_{6s^1 5d^1}(^3D)$ + Rb^+ channel (see Figure 1 and Table 5).

The expected fast non-radiative charge transfer to the $^3\Pi_{1,0^-}$ states may, however, not be experimentally desirable since it will irreversibly 'destroy' the Ba ion. This finding is in great contrast to what is observed in the valence isoelectronic system $(NaCa)^+$. Here, a radiative lifetime of charge transfer in the order of 10^4 s to 10^6 s for the $A\ ^1\Sigma^+$ to the $X\ ^1\Sigma^+$ was calculated by Makarov *et. al* [10]. The $A\ ^1\Sigma^+$ (and most likely also the $a\ ^3\Sigma^+$) electronic states of $(NaCa)^+$ are thus very long-lived metastable species. This occurs since there are no close-lying P states mixing into the excited Σ states, making both radiative transitions electric dipole forbidden and for the $a\ ^3\Sigma^+$ also spin forbidden. With the transition dipole moments at hand it would be possible to go from the present qualitative analysis to more quantitative predictions of life times for the excited states in $(RbBa)^+$. This is clearly of interest, and has prompted us to start the development of a MRCI transition dipole moment module [20, 44].

Furthermore, at an internuclear distance of 15 to 16 bohr we see the $^1\Sigma^+$ excited state of the entrance channel crossing the $\Omega = 0^+$ of the $^3\Pi$ state (see Figure 1). While

one normally would not expect two $\Omega = 0^+$ states to cross, however, for this 15-16 bohr electron-transfer process the off diagonal element between the two states is so small that we cannot visibly see any effect of it. Compared with this, a clear avoided crossing in the 12 to 13 bohr range between the $^1\Sigma^+$ and the higher lying $\Omega = 0^+$ of a $^1\Sigma^+$ from the $Ba_{6s^15d^1}(^1D)$ but also $\Omega = 0^+$ of a $^3\Pi$ of the $Ba_{6s^16p^1}(^3P)$ is observed. This avoided crossing helps making the $^1\Sigma^+$ of the entrance channel a metastable state which is in contrast to what is observed in the lighter homologous where this is a dissociative state.

As seen from Table 5 the Ω components of the $^3\Delta$ state are markedly split by spin-orbit interaction, but display equal equilibrium bond distances. The irregular splitting pattern of the $^3\Delta$ fine-structure levels reveals in this context substantial off-diagonal spin-orbit coupling of the $\Omega = 2$ component with the close-by $^1\Delta$ state. The $^3\Sigma^+$ and $^1\Sigma^+$ states originating from the $Ba_{6s^15d^1}(^3D)$ channel $Ba_{6s^15d^1}(^1D)$ channels, respectively, exhibit very irregular behavior due to avoided crossings. Moreover, at short internuclear distances in the same energy regime additional states that correlate with higher dissociation channels are found that are not represented properly in our calculations. It is therefore not meaningful to discuss the electronic structure of these higher-lying $^3\Sigma^+$ and $^1\Sigma^+$ states.

3.4. Dipole moment

Finally, we show in Figure 3 the dipole moment curve of the molecular ground state of $(RbBa)^+$ calculated at the four-component CCSD(T) level with origin at the center of mass. The corresponding curve at the CCSD level (not shown) is almost identical, supporting that the CCSD(T) curve is converged. A charge distribution corresponding purely to Rb^+ and Ba would yield a dipole moment around 14 Debye at the calculated equilibrium distance of 8.75 bohr (see Fig. 3). Due to a partial electron transfer from Ba to Rb^+ (*cf.* discussion in section 3.2), the dipole moment of the electronic ground state is significantly lower. As seen in Table 6 we calculate a vibrationally averaged dipole moment of 4.53 Debye at our best level, the counterpoise corrected CCSD(T). Since the dipole moment function is almost linear in the region of the rovibrational ground state wave function, we only see a minor difference between the vibrationally averaged dipole moment and the dipole moment taken at the electronic equilibrium distance as shown in Table 6. Naturally, when the internuclear distance is increased the dipole moment converges asymptotically towards the dipole moment one would calculate by replacing the wave function with a unit point charge for Rb^+ and zero point charge for Ba.

4. Summary and Prospects

The objective of this study has been to form a firm basis for design of ultracold experiments with low-energy collisions of Ba^+ with Rb. At large internuclear distances the potential energy of a diatomic molecule can be calculated accurately by perturbation theory from the properties of its separated atoms alone [45]. We therefore here focused

on the short-range part of the low-lying electronic states.

The $(RbBa)^+$ ground state is found to form a partially covalent polar bond and therefore stronger than was expected *a priori*. While the dissociation energy is comparable to the LiCs alkali dimer, the harmonic frequency is only one third of the LiCs value, indicating that the two bonds are significantly different. The broader $(RbBa)^+$ potential displays the longer ranging charge induced dipole interaction against the neutral dissociation of LiCs. We furthermore show that the electronic ground state possesses a dipole moment significantly smaller than from a pure charge-dipole interaction. We attribute this finding to a partial charge transfer from Ba to Rb^+, which was also supported by a Mulliken population analysis.

As barium is a special case among the alkaline earth metals because of its low-lying ^{1,3}D states, it presents a unique opportunity to study non-radiative charge-transfer processes in the excited-state manifold of $(RbBa)^+$ that will be formed in ultracold collision experiments of Rb + Ba^+. The non-adiabatic interaction between the $^3\Sigma^+$ and $^3\Pi$ excited states is in particular anticipated to have significant impact on the above mentioned process. In the Ba^+ + Rb entrance channel the system is prepared initially in a highly-excited vibrational level of the $^3\Sigma^+$ potential. At short internuclear separation the non-adiabatic interaction yields a finite probability for a non-radiative transition to the $^3\Pi$ potential which in turn can relax to the electronic ground state by emission of a photon. First, the transition to $^1\Sigma^+_{0^+}$ ground state is formally spin forbidden, however, due to the significant spin-orbit coupling in the $^3\Pi$ state this prohibition is lifted. Second, the calculated large admixture of the of Ba $6p_\pi$ and Rb $5p_\pi$ spinors with the Ba $5d_\pi$ spinor must significantly increase the electric dipole transition strength. We therefore expect the lifetime of the $^3\Pi$ states to be significantly reduced compared to the non-relativistic analysis. Moreover, we identified a metastable $^1\Sigma^+$ excited state which may experimentally provide access to the creation of a mesoscopic molecular bound state starting from a Bose-Einstein condensate of Rb atoms and trapped Ba^+ ions.

As a consequence of this study we have demonstrated the capability of the relativistic all-electron quantum-chemical methodology [30, 15, 19] to yield accurate ground and excited states. We have shown that these methods are capable of handling both neutral and complex ionized systems from the atomic limit all the way to the short range potential. This is seen from the accurate differential ionization potential ΔIP, atomic excitation energies, and fine structure splittings; this was only possible because of the ability to handle the complicated excited-state potentials of highly multiconfigurational open-shell character. We have shown that our chosen MRCI model is adequate for these purposes and furthermore reproduces the accurate CCSD(T) data for the spectroscopic properties of the ground state.

All used codes except the MRCI code are released in the DIRAC08[28] program package. The parallelized MRCI code will be made available in the forthcoming release of DIRAC, thus making it possible for other researchers to perform such accurate calculations, for example on other diatomic molecules of potential interest in ultracold experiments.

Acknowledgments

Financial support of this project by the Deutsche Forschungsgemeinschaft (reference number FL 256/5-1), SFB 663 and through the priority program SPP 1145, grant no. FL 356/2 is gratefully acknowledged. A generous allotment of computing time from the Danish Center for Scientific Computing is gratefully acknowledged. Further computational support and infrastructure was provided by the "Zentrum fuer Informations- und Medientechnologie" (ZIM) at the Heinrich Heine University Düsseldorf (Germany).

Table 1. Spectroscopic values for the $\Omega = 0^+$ ground state calculated with the spinfree (SF) CCSD and CCSD(T) methods, with an energy truncation threshold for active virtual spinors at 18 and 42 Hartree, and using the Visscher small component approximation[46] for the $\langle SS|SS\rangle$ integrals.

Method	Virtuals truncation	R_e[bohr]	ω_e [cm^{-1}]
SF-CCSD	18	8.8027	52.179
SF-CCSD	42	8.8025	52.179
SF-CCSD(T)	18	8.7528	52.794
SF-CCSD(T)	42	8.7526	52.795

Table 2. A selection of molecular electronic states in the $\Lambda - S$ coupling picture and associated atomic dissociation channels in an energy range of up to ≈ 14000 cm^{-1}.

Atomic $^{(2S+1)}L_J$	Molecular $^{(2S+1)}\Lambda_\Omega$
$Rb^+_{5s^0}$ ($^1S_0$) + Ba_{6s^2} ($^1S_0$)	$^1\Sigma^+_{0^+}$
Rb_{5s^1} ($^2S_{1/2}$) + $Ba^+_{6s^1}$ ($^2S_{1/2}$)	$^3\Sigma^+_{1,0^-}$, $^1\Sigma^+_{0^+}$
$Rb^+_{5s^0}$ ($^1S_0$) + $Ba_{6s^15d^1}$ ($^3D_{1,2,3}$)	$^3\Delta_{3,2,1}$, $^3\Pi_{2,1,0^+,0^-}$, $^3\Sigma^+_{1,0^-}$
$Rb^+_{5s^0}$ ($^1S_0$) + $Ba_{6s^15d^1}$ ($^1D_2$)	$^1\Delta_2$, $^1\Pi_1$, $^1\Sigma^+_{0^+}$
$Rb^+_{5s^0}$ ($^1S_0$) + $Ba_{6s^16p^1}$ ($^3P_{0,1,2}$)	$^3\Pi_{2,1,0^+,0^-}$, $^3\Sigma^+_{1,0^-}$

Table 3. Excitation energies T in cm^{-1} for the lowest $Ba_{6s^2}(^1S_0) \rightarrow Ba_{6s^15d^1}(^3D_{1,2,3})$, $Ba_{6s^2}(^1S_0) \rightarrow Ba_{6s^15d^1}(^1D_2)$ and $Ba_{6s^2}(^1S_0) \rightarrow Ba_{6s^16p^1}(^3P_{0,1,2})$, electronic transitions calculated at the atomic MRCI S6_(2in9)_SD and atomic-like S12_(2in13)_SD (molecular calculation; values taken at $R = 50$ bohr) levels. The active space in the atomic calculation includes the same Ba shells and the same truncation threshold for the virtual spinors as in the molecular case. Details on the molecular computational level are given in the text. The MRCI results are compared to previous theoretical and experimental data. In the atomic-like "J states" (Ω) the individual M_J components are almost degenerate at $R = 50$ bohr with deviations on the order of $4 - 8$ cm^{-1} from the lowest to highest M_J component. We here show the energies of the lowest M_J values in the table.

	$^1S_0$		$^3D_{1,2,3}$		$^1D_2$	$^3P_{0,1,2}$		
Method	$J = 0$	$J = 1$	$J = 2$	$J = 3$	$J = 2$	$J = 0$	$J = 1$	$J = 2$
Experiment [47]	0	9034	9216	9597	11395	12266	12637	13515
Atomic calculations								
S6_(2in9)_SD	0	8627	8809	9175	11197	12732	13091	13944
FSCCSD [40]	0	9075	9260	9639	11621	12423	12802	13793
IHFSCCSD [40]	0	9117	9296	9677	11426	12397	12728	13610
Molecular calculation at $R = 50$ bohr								
S12_(2in13)_SD	0	8619	8812	9174	11198	12736	13109	13936

Table 4. Spectroscopic values for the $\Omega = 0^+$ ground state calculated at the spin-dependent MRCI S12_(2in13)_SD level in comparison to CC results, both at the spinfree (SF) and spin-dependent levels, and results from earlier spinfree MRCI SF-SD16_(2in7)_SD calculations where an ANO-RCC basis was used along with a truncation of the virtual space at 5 Hartree. Counterpoise corrections ("cp-" prefix) have also been tested.

Method	R_e[bohr]	ω_e [cm^{-1}]	D_e [cm^{-1}]
SF-SD16_(2in7)_SD [15]	8.75	54.327	5509
S12_(2in13)_SD	8.72	51.773	5055
SF-CCSD	8.80	52.171	4887
CCSD	8.80	52.187	4886
SF-CCSD(T)	8.75	52.785	5035
CCSD(T)	8.75	52.799	5034
cp-SF-CCSD	8.81	52.145	4877
cp-CCSD	8.80	52.161	4876
cp-SF-CCSD(T)	8.76	52.755	5023
cp-CCSD(T)	8.76	52.768	5022

Table 5. Spectroscopic constants for the ground and lowest excited states (Ω designation) of $(RbBa)^+$ calculated at the MRCI S12_(2in13)_SD level with 14 explicitly correlated electrons.

State	Ω	$\Lambda - S^a$	R_e [bohr]	ω_e [cm^{-1}]	D_e [cm^{-1}]	T_v [cm^{-1}]	T_e [cm^{-1}]
1	0^+	$^1\Sigma^+$	8.72	52	5055	0	0
2	0^-	$^3\Sigma^+$	9.22	45	6889	6711	6621
3	1	$^3\Sigma^+$	9.22	45	6871	6737	6638
4	0^+	$^3\Pi$	8.28	52	5899	7865	7775
5	0^-	$^3\Pi$	8.40	53	5980	7939	7878
6	1	$^3\Pi$	8.28	56	5742	8022	7932
7	2	$^3\Pi$	8.28	52	6702	8109	8033
8	1	$^3\Delta$	9.22	43	4302	9653	9556
9	2	$^3\Delta$	9.22	43	4500	9809	9721
10	3	$^3\Delta$	9.22	43	4157	10165	10064
11	2	$^1\Delta$	9.22	43	5887	10440	10365
12	1	$^3\Sigma^+$	9.22	37	2258	12047	11963
13	0^-	$^3\Sigma^+$	9.03	44	2216	12053	12005
14	0^+	$^1\Sigma^+$	9.77	39	-	13030	12601
15	1	$^1\Pi$	9.72	40	3566	13112	12687

[a] leading $\Lambda - S$ projection

Table 6. Dipole moments at R_e (μ_e) and the vibrationally averaged dipole moment μ_v for the CCSD and CCSD(T) levels of theory and with counterpoise ("cp-" prefix) corrected values.

Method	μ_e [D]	μ_v [D]
SF-CCSD	4.528	4.550
cp-SF-CCSD	4.533	4.556
SF-CCSD(T)	4.507	4.528
cp-SF-CCSD(T)	4.514	4.534

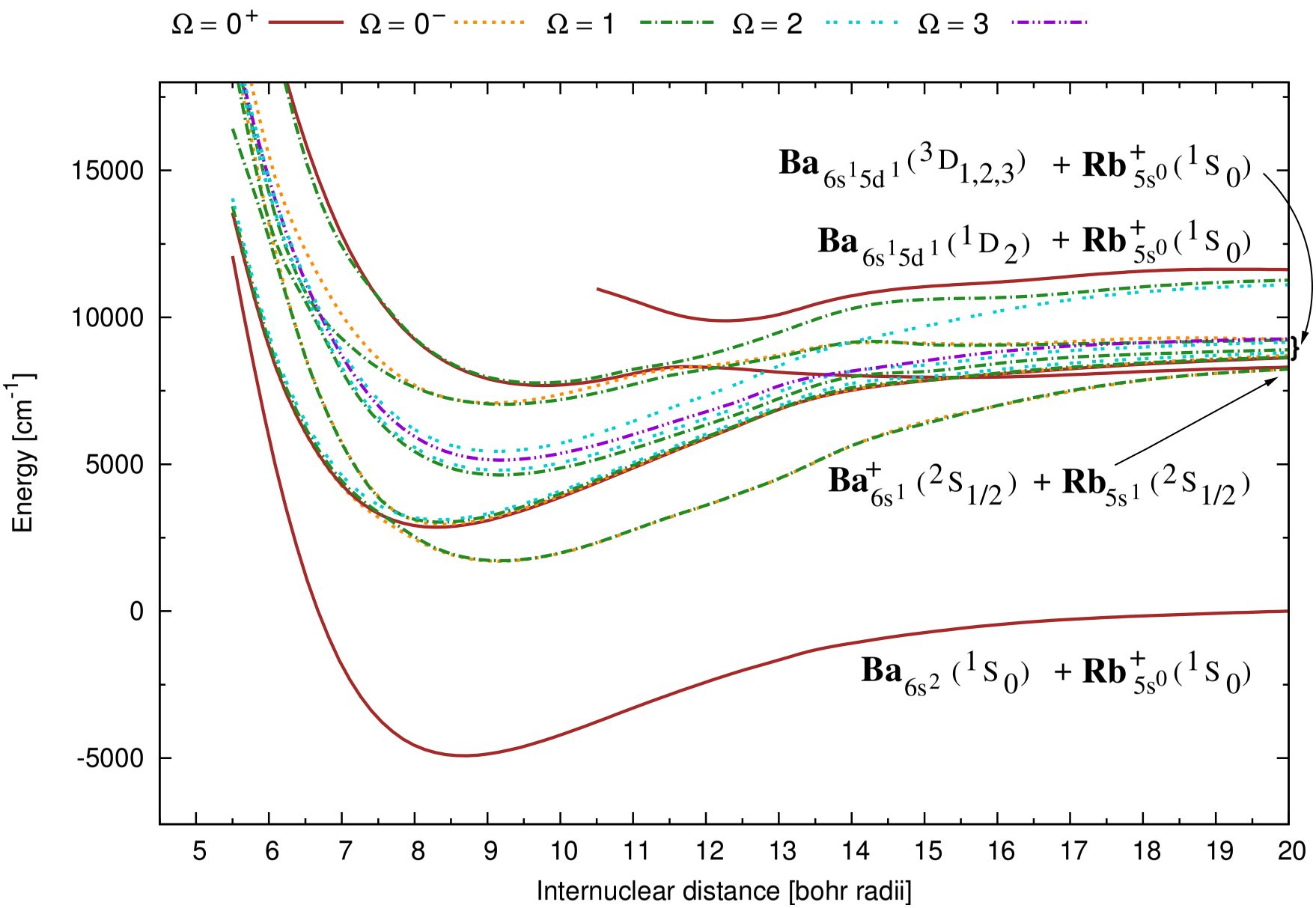

Figure 1. Potential energy curves of the ground and low-lying states (Ω designation) of $(RbBa)^+$ computed at the four-component MRCI S12_(2in13)_SD level (see text for more details). Atomic dissociation channels for the states are indicated in the picture (see Table 2 for details).

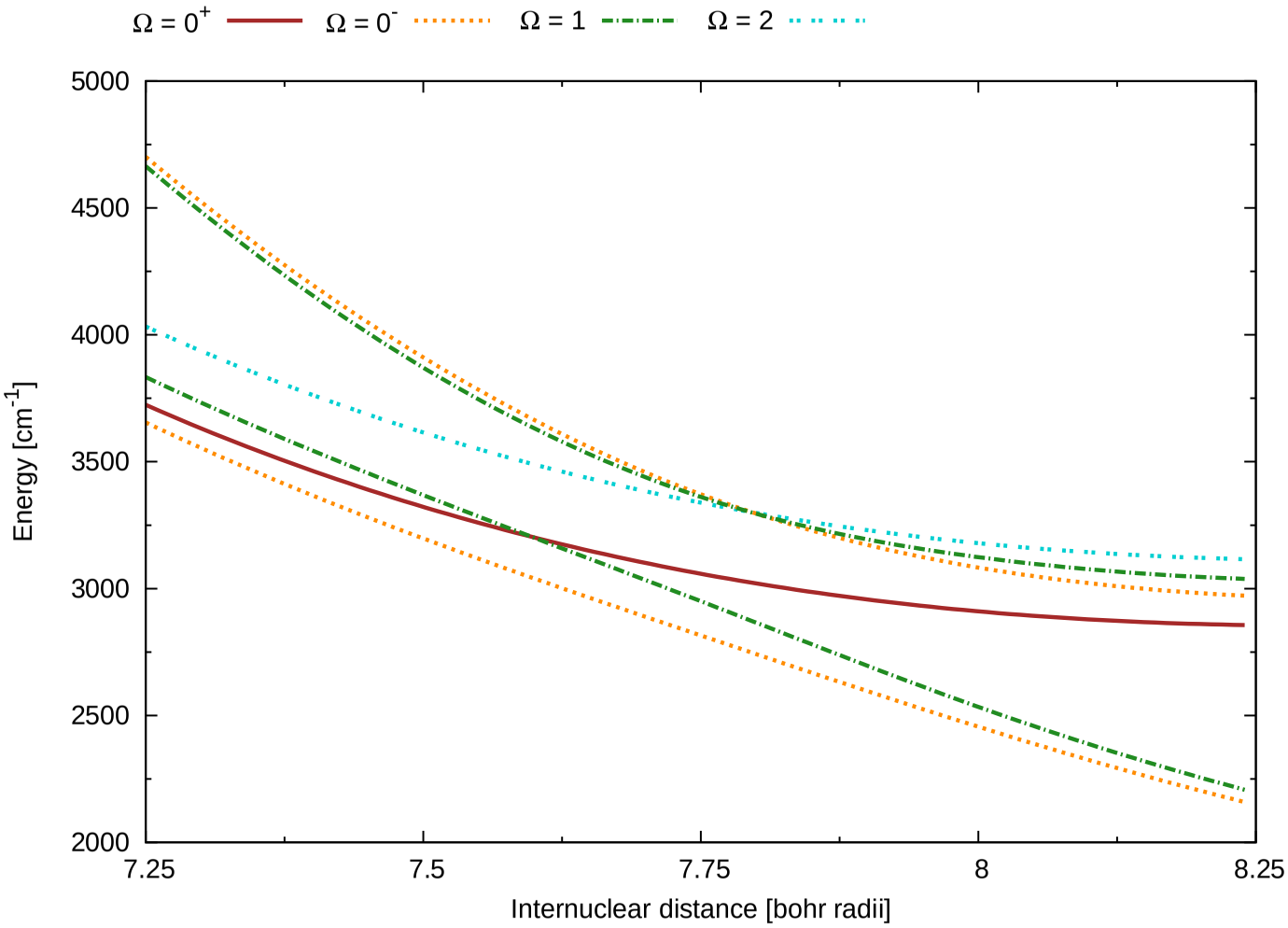

Figure 2. Close up of the avoided crossings between the $^3\Sigma^+_{1,0^-}$ Rb + Ba^+ entrance channels and and low-lying charge transfer $^3\Pi_{1,0^-}$ states of the Rb^+ and $Ba_{6s^1 5d^1}$ (^{3}D) atomic channels.

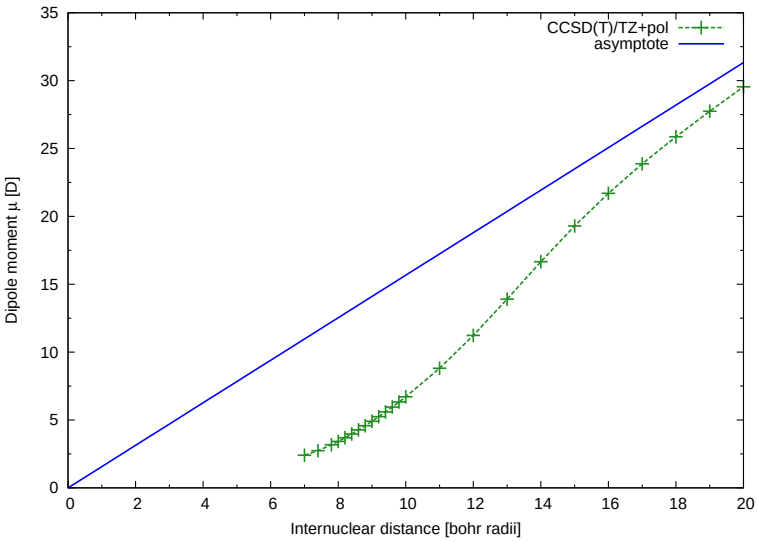

Figure 3. Four-component CCSD(T) dipole moment curve (in Debye) of the molecular ground state calculated with 14 explicitly correlated electrons. The straight line (blue) indicates the asymptotic limit of the dipole moment μ for a charged system in the center-of-mass coordinates.

[1] J Doyle, B Friedrich, R V Krems, and F Masnou-Seeuws. Quo vadis, cold molecules? *Eur. Phys. J. D*, 31:149, 2004.

[2] J J Hudson, B E Sauer, M R Tarbutt, and E A Hinds. Measurement of the electron electric dipole moment using YbF molecules. *Phys. Rev. Lett.*, 89:023003, 2002.

[3] B C Regan, E D Commins, C J Schmidt, and D DeMille. New limit on the electron electric dipole moment. *Phys. Rev. Lett.*, 88:071805, 2002.

[4] S Schiller and V Korobov. Tests of time independence of the electron and nuclear masses with ultracold molecules. *Phys. Rev. A*, 71:032505, 2005.

[5] E Bodo and F A Gianturco. Ultra low-energy behavior of an ionic replacement reaction ^{3}He^{4}He$^+ + {}^4$He $\rightarrow {}^4$He$_2^+ + {}^3$He. *Phys. Rev. A*, 73:032702, 2006.

[6] M. Leduc and J. Vigué. Interplay between theoretical quantum chemistry and cold atom experiments. *Theoret. Chim. Acta*, 116:598, 2006.

[7] R Côté and A Dalgarno. Ultracold atom-ion collisions. *Phys. Rev. A*, 62:012709, 2000.

[8] P E Siska. Cold and ultracold ion-neutral inelastic collisions: Spin-orbit relaxation in He + Ne$^+$. *J. Chem. Phys.*, 115:4527, 2001.

[9] E Wells, K D Carnes, B D Esry, and I Ben-Itzhak. Charge transfer and elastic scattering in very slow H$^+$+D(1s) half collisions. *Phys. Rev. Lett.*, 86:4803, 2001.

[10] O. P. Makarov, R. Côté, H. Michels, and W. W. Smith. Radiative charge-transfer lifetime of the excited state of $(NaCa)^+$. *Phys. Rev. A*, 67:042705, 2003.

[11] R. Coté, V. Kharchenko, and M. D. Lukin. Mesocopic molecular ions in Bose-Einstein condensates. *Phys. Rev. Lett.*, 89:093001, 2002.

[12] J. Hecker Denschlag. University of Innsbruck (now University of Ulm), private communication, 2009. Project BaRbIe: An ion in a sea of ultracold neutral atoms, see also http://www.uibk.ac.at/exphys/ultracold/projects/barbi/index.html.

[13] M. Sabidó, J. de Andrés, J. Sogas, M. Alberti, J. M. Bofill, and A. Aguilar. Inelastic electronic excitation and electron transfer processes in collisions between Mg(3^1S$_0$) atoms and K$^+$(^{1}S$_0$) ions studied by crossed beams in the 0.10-3.80-kev energy range. *J. Chem. Phys.*, 123:124314, 2005.

[14] M. Sabidó, J. de Andrés, J. Sogas, M. Alberti, J. M. Bofill, and A. Aguilar. Crossed ion-atom beam study of the inelastic collision processes between neutral Mg(3^1S$_0$) atoms and Cs$^+$(^{1}S$_0$) ions in the 0.05-4.20 kev energy range. *Phys. Chem. Chem. Phys.*, 7:310, 2005.

[15] S Knecht, H J Aa Jensen, and T Fleig. Large-scale parallel configuration interaction. I. Nonrelativistic and scalar-relativistic general active space implementation with application to (Rb-Ba)$^+$. *J. Chem. Phys.*, 128:014108, 2008.

[16] K G Dyall. An exact separation of the spin-free and spin-dependent terms of the Dirac-Coulomb-Breit Hamiltonian. *J. Chem. Phys.*, 100:2118, 1994.

[17] W. Kutzelnigg. Basis set expansion of the Dirac operator without variational collapse. *Int. J. Quantum Chem.*, 25:107, 1984.

[18] L Visscher and T Saue. Approximate relativistic electronic structure methods based on the quaternion modified Dirac equation. *J. Chem. Phys.*, 113:3996, 2000.

[19] S Knecht, H J Aa Jensen, and T Fleig. Large-scale parallel configuration interaction. II. Two- and four-component double-group general active space implementation with application to BiH, 2009. revised manuscript submitted.

[20] Stefan R. Knecht. *Parallel Relativistic Multiconfiguration Methods: New Powerful Tools for Heavy-Element Electronic-Structure Studies.* Dissertation, Mathematisch-Naturwissenschaftliche Fakultät, Heinrich-Heine-Universität Düsseldorf, 2009. http://docserv.uni-duesseldorf.de/servlets/DocumentServlet?id=13226.

[21] T Fleig, J Olsen, and C M Marian. The generalized active space concept for the relativistic treatment of electron correlation. I. Kramers-restricted two-component configuration interaction. *J. Chem. Phys.*, 114:4775, 2001.

[22] T Fleig, J Olsen, and L Visscher. The generalized active space concept for the relativistic

treatment of electron correlation. II: Large-scale configuration interaction implementation based on relativistic 2- and 4-spinors and its application. *J. Chem. Phys.*, 119:2963, 2003.

[23] T Fleig, H J Aa Jensen, J Olsen, and L Visscher. The generalized active space concept for the relativistic treatment of electron correlation. III: Large-scale configuration interaction and multi-configuration self-consistent-field four-component methods with application to UO_2. *J. Chem. Phys.*, 124:104106, 2006.

[24] R J Bartlett and M Musial. Coupled-cluster theory in quantum chemistry. *Rev. Mod. Phys.*, 79:291, 2007.

[25] E R Davidson. The iterative calculation of a few of the lowest eigenvalues and corresponding eigenvectors of large real-symmetric matrices. *J. Comput. Phys.*, 17:87, 1975.

[26] J Olsen, P Jørgensen, and J Simons. Passing the one-billion limit in full configuration interaction (FCI) calculations. *Chem. Phys. Lett.*, 169:463, 1990.

[27] E R Davidson. Monster matrices: their eigenvalues and eigenvectors. *Computer in Physics*, 7:519–522, 1993.

[28] DIRAC, a relativistic ab initio electronic structure program, Release DIRAC08 (2008), written by L. Visscher, H. J. Aa. Jensen, and T. Saue, with new contributions from R. Bast, S. Dubillard, K. G. Dyall, U. Ekström, E. Eliav, T. Fleig, A. S. P. Gomes, T. U. Helgaker, J. Henriksson, M. Iliaš, Ch. R. Jacob, S. Knecht, P. Norman, J. Olsen, M. Pernpointner, K. Ruud, P. Sałek, and J. Sikkema (see http://dirac.chem.sdu.dk).

[29] L Visscher, K G Dyall, and T J Lee. Kramers-restricted closed-shell CCSD theory. *Int. J. Quantum Chem.: Quantum Chem. Symp.*, 29:411, 1995.

[30] L Visscher, T J Lee, and K G Dyall. Formulation and implementation of a relativistic unrestricted coupled-cluster method including noniterative connected triples. *J. Chem. Phys.*, 105:8769, 1996.

[31] L K Sørensen, T Fleig, and J Olsen. Spectroscopic and electric properties of the LiCs molecule. A coupled cluster study including higher excitations. *J. Phys. B*, 42:165102, 2009.

[32] L. K. Sørensen, S. Knecht, T. Fleig, and C. M. Marian. Four-component relativistic coupled cluster and configuration interaction calculations on the ground and excited states of the RbYb molecule. *J. Phys. Chem. A*, 113:12607, 2009.

[33] G. F. Gribakin and V. V. Flambaum. Calculation of the scattering length in atomic collisions using the semiclassical approximation. *Phys. Rev. A*, 48(1):546–553, 1993.

[34] K.G. Dyall. Relativistic double-zeta, triple-zeta, and quadruple-zeta basis sets for the 4s, 5s, 6s, and 7s elements. *J. Phys. Chem. A*, 113:12638, 2009.

[35] I. S. Lim, H. Stoll, and P. Schwerdtfeger. Relativistic small-core energy-consistent pseudopotentials for the alkaline-earth elements from Ca to Ra. *J. Chem. Phys.*, 124:034107, 2006.

[36] S F Boys and F Bernardi. The calculation of small molecular interactions by the differences of separate total energies. Some procedures with reduced errors. *Mol. Phys.*, 19:553, 1970.

[37] Andrzej Sadlej. Program WFFIT. University of Torun.

[38] C. W. Bauschlicher Jr., S. P. Walch, and H. Partridge. On correlation in the first row transition metal atoms. *J. Chem. Phys.*, 76:1033–1039, 1982.

[39] L. Visscher, E. Eliav, and U. Kaldor. Formulation and implementation of the relativistic Fock-space coupled cluster method for molecules. *J. Chem. Phys.*, 115(21):9720–9726, 2001.

[40] A. Landau, E. Eliav, Y. Ishikawa, and U. Kaldor. Intermediate Hamiltonian Fock-space coupled-cluster method: Excitation energies of barium and radium. *J. Chem. Phys.*, 113:9905–9910, 2000.

[41] A. Landau, E. Eliav, Y. Ishikawa, and U. Kaldor. Intermediate Hamiltonian Fock-space coupled cluster method in the one-hole one-particle sector: Excitation energies of xenon and radon. *J. Chem. Phys.*, 115:6862–6865, 2001.

[42] *NIST Chemistry WebBook* (version 69, 2005) National Institute of Standards and Technology, Gaithersburg, MD.

[43] P Staanum, A Pashov, H Knöckel, and E Tiemann. $X^1\Sigma^+$ and $a^3\Sigma^+$ states of LiCs studied by

Fourier-transform spectroscopy. *Phys. Rev. A*, 75:042513, 2007.

[44] S. Knecht and H. J. Aa Jensen. A general-purpose parallel four-component Kramers-restricted CI property module. unpublished work.

[45] W C Stwalley and H Wang. Photoassociation of ultracold atoms: A new spectroscopic technique. *J. Mol. Spectrosc.*, 195:194, 1999.

[46] L Visscher. Approximate molecular relativistic Dirac-Coulomb calculations using a simple Coulombic correction. *Theoret. Chem. Acc.*, 98:68, 1997.

[47] Y. Ralchenko, A. E. Kramida, J. Reader, and NIST ASD Team (2008). NIST Atomic Spectra Database (version 3.1.5). Available: http://physics.nist.gov/asd3 (retrieved May 3rd, 2009). National Institute of Standards and Technology, Gaithersburg, MD.